Inorganic Chemistry

Article

pubs.acs.org/IC

Structures of d^4 MH_3X: a Computational Study of the Influence of the Metal and the Ligands

Amalia I. Poblador-Bahamonde, Christophe Raynaud,* and Odile Eisenstein*

Institut Charles Gerhardt, Université Montpellier 2, CNRS 5253, cc 1501, Place Eugène Bataillon, 34095 Montpellier, France

Supporting Information

ABSTRACT: Density functional theory (DFT, PBE0, and range separated DFT, RSH + MP2) and coupled-cluster with single and double and perturbative triple excitations (CCSD-(T)) calculations have been used to probe the structural preference of d^4 MH_3X^q (M = Ru, Os, Rh^+, Ir^+, and Re^-; X = H, F, CH_3, CF_3, SiH_3, and SiF_3) and of MX_4 (M = Ru; X = H, F, CH_3, CF_3, SiH_3, and SiF_3). Landis et al. have shown that complexes in which the metal is sd^3 hybridized have tetrahedral and non-tetrahedral structures with shapes of an umbrella or a 4-legged piano stool. In this article, the influence of the metal and ligands on the energies of the three isomeric structures of d^4 MH_3X and MX_4 is established and rationalized. Fluoride and alkyl ligands stabilize the tetrahedral relative to non-tetrahedral structures while hydride and silyl ligands stabilize the non-tetrahedral structures. For given ligands and charge, 4d metal favors more the non-tetrahedral structures than 5d metals. A positive charge increases the preference for the non-tetrahedral structures while a negative charge increases the preference for the tetrahedral structure. The factors that determine these energy patterns are discussed by means of a molecular orbital analysis, based on Extended Hückel (EHT) calculations, and by means of Natural Bond Orbital (NBO) analyses of charges and resonance structures (NRT analysis). These analyses show the presence of through-space interactions in the non-tetrahedral structures that can be sufficiently stabilizing, for specific metals and ligands, to stabilize the non-tetrahedral structures relative to the tetrahedral isomer.

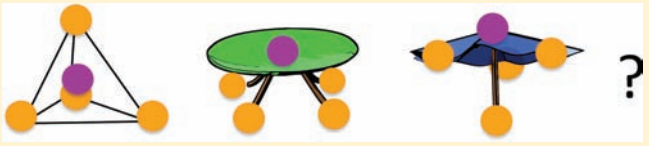

INTRODUCTION

Unsaturated transition metal complexes are a model of reactive intermediates, and their structures and electronic properties can provide useful information on how they could react. These species are often very reactive and hard to characterize by experimental means. Therefore, structure and bonding analyses and computational studies have been useful to establish the structures of these complexes. The structure of unsaturated species does not always follow the rules that apply for saturated systems. For instance, it has been found that the structure of unsaturated species cannot be always predicted by the valence shell electron pair repulsion (VSEPR) theory[1] or by a simple ionic model. WMe_6 and WH_6 are notable cases for the failure of the VSEPR theory since they have distorted trigonal prismatic structures with C_{3v} symmetry[2] while VSEPR would have predicted an octahedral coordination. The VSEPR also fails to predict the bent structure of molecular dihalides of the heavy alkaline earth metals (Ca, Sr, and Ba) and the pyramidal structure of trihydrido complexes such as ScH_3, LaH_3, TiH_3^+, ZrH_3^+, and their alkyl analogues. These species and related d^0 complexes have been described in a comprehensive review.[3] The main feature that emerges from the studies is that distortion away from the structure predicted by VSEPR is prevalent for complexes with hydride or alkyl ligands, which have no π-donor capability, while the presence of π-donor ligand like halide lead more often to structures that follow the VSEPR rule. For instance, WCl_6 is octahedral[4] while WMe_6 and WH_6 are not. Analysis of the metal−ligand bonding within such complexes shows that the electron delocalization between the π-donor ligand and the formally empty metal d orbital increases the electron density at the metal which, in turn, becomes less unsaturated. Therefore, the structures of polyhydride or polyalkyl complexes are considered as informative of the fundamental structural preferences associated with the metal coordination number and the number of d electrons. Unfortunately, few systems of this type have been characterized experimentally, a clear consequence of the poor stability of highly unsaturated species. For this reason, computational studies have been widely used.[5]

Landis et al. have shown that valence bond concepts can be used for describing the shape of a variety of hydride and alkyl systems.[6] A primary feature of their studies is that the valence empty $(n + 1)$p orbitals of a nd metal do not contribute to the metal−ligand bonds, which are constructed from the $(n + 1)$s and available nd orbitals.[7] Consequently, the shape of the hydride complex, where the metal has λ nonbonding electron pairs, is determined by the optimal spatial distribution of the sd^ω ($\omega = 5 - \lambda$) hybrids set, that is, the spatial distribution that minimizes the interactions between the hybrid orbitals. In general, there is more than one optimal spatial distribution for a given sd^ω set and quantum calculations are used to determine the relative energies of these isomeric structures.[7a,8,9] Similar results were obtained using the orbitally ranked symmetry

Received: January 19, 2012
Published: May 7, 2012

   dx.doi.org/10.1021/ic3001448 | *Inorg. Chem.* 2012, 51, 5705−5715

analysis method (ORSAM) since for low coordinated complexes the metal orbital uses also the $(n + 1)$s and nd orbitals and the ranking of the structures is also done by quantum calculations.[10] In these studies, only hydride complexes were calculated but other ligands were not explicitly considered. Likewise the influence of the metal was not explored.

Well-defined experimental species are rather limited since the only known complexes of this type are the homoleptic neutral (M = Ru and Os) and cationic (M = Ir^+) d^4 MR_4 (R = alkyl and aryl) complexes synthesized by Wilkinson. These complexes, $Ru(C_6H_{11})_4$,[11] $Ru(o\text{-}Tolyl)_4$,[12] $Ru(Mesityl)_4$,[13] $Os(C_6H_{11})_4$,[11] $Os(o\text{-}Tolyl)_4$,[14] and $Ir(Mesityl)_4^+$,[13] are stable and have a tetrahedral coordination at the metal. However, the bonding analysis of Landis and the ORSAM analysis of Hall predict that other isomers with non-tetrahedral structures should be possible, and calculations for RuH_4 and OsH_4 have shown that non-tetrahedral structures could even be preferred or at least competitive, but no rationale for these results is available. We were intrigued by these results, and we wanted to explore more widely the structural preferences of d^4 MH_3X and MX_4 for various metals, charges, and ligands. We present a study based on density functional theory (DFT) calculations, validated by ab initio calculations, for neutral MH_3X (M = Ru and Os; X = H, F, CF_3, CH_3, SiF_3, and SiH_3), cationic $[MH_3X]^+$ (M = Rh and Ir), and anionic $[ReH_3X]^-$ complexes. We also present results for homoleptic RuX_4 (X = H, F, CH_3, CF_3, SiH_3, and SiF_3) complexes.

COMPUTATIONAL METHODS

Two methods (1 and 2) were used to obtain the geometries and energies at the DFT level. Additional methods were used to increase the accuracy of the relative energies of the isomers, methods 3 and 4. The validity of the DFT method was established with method 5.

Method 1. The geometry optimizations were performed at the DFT level of theory with Gaussian 09[15] using the B3PW91 functional.[16] The metal centers were described with the Stuttgart/Dresden (SDD) quasi-relativistic effective core potentials (RECP) and the associated basis sets.[17] The 6-31G(d,p) basis set were used for the other atoms.[18]

Method 2. The geometries obtained with the method 1 were used as initial input for optimization with the PBE0 functional[19] and triple-ζ quality basis sets on all atoms, def2-TZVPP,[20] with the corresponding RECP for the metal.[21] With rare exceptions, the optimized structures obtained with method 2, and method 1 are similar. Bond lengths only differ by about 0.01 Å, and bond angles differ by less than 5°. The structures and energies obtained with method 2 are used for describing the results in this Article. All stationary points were fully characterized by analytical frequency calculations as either a minimum or a transition state. Intrinsic reaction coordinate (IRC) calculations followed by geometry optimizations were used to associate a transition state to the corresponding two minima. The energies reported in this article do not include the ZPE correction, but it has been verified that the ZPE correction does not modify significantly the relative energies of the isomers. The optimized geometries for all stationary points and the ZPE corrected energies are given in the Supporting Information.

Method 3. Single-point short-range (sr-) DFT/long-range (lr-) ab initio calculations on the DFT (PBE0/def2-TZVPP) geometries were carried out for all structures using the Molpro 2010.1 program.[22] The short-range exchange-correlation terms were treated by the sr-PBE variant functional.[23] The long-range portion of the exchange energy is explicitly treated (HF). This step defines a "range-separated hybrid" (RSH) scheme, which is corrected in a second step for the long-range correlation effects by a second order perturbation theory, leading to MP2-like correction. This method is referred to as RSH+MP2.[24] The range-separation parameter μ has been set to 0.4 a_0^{-1}. For these single-point calculations, all atoms were described with quadruple-ζ quality basis sets, def2-QZVPP[25] with the corresponding RECP for the metal.[21]

Method 4. Single-point coupled-cluster with single and double and perturbative triple excitations (CCSD(T)) calculations on the DFT (PBE0/def2-TZVPP) optimized geometries were carried out for MH_3X (M = Ru and Os; X = H, F, CF_3, CH_3, SiH_3, and SiF_3) using the Orca 2.9 program.[26] In this case, all atoms were described with def2-QZVPP[25] basis sets with the corresponding RECP for the metal.[21]

Method 5. Single-point MR-CI and MR-ACPF-2a[27] calculations on the DFT (PBE0/def2-TZVPP) optimized geometries were carried out for RuH_4 using the Orca 2.9 program.[26] In this case, all atoms were described with a def2-QZVPP[25] basis sets with the corresponding RECP for the metal.[21] Resolution of the identity (RI) approximation was used for the integral transformation with def2-QZVPP/C auxiliary basis sets.[28] For these MRCI and MR-ACPF-2a calculations, the reference space was built from full valence CASSCF orbitals (12 electrons, 10 orbitals) using a selection threshold (Tpre) set to 10^{-6}. The selection of the excited configurations from the reference space was done with a selection threshold (Tsel) of 10^{-9}. The effect of the rejected configurations was estimated using second order perturbation theory.

Analysis of the Results. The Extended Hückel (EHT) calculations were carried out with the Yaehmop program.[29] The Ru 4d, 5s, and 5p orbitals are −14.9, −10.4, and −6.87 eV, respectively.[30] The energy of the "normal" hydrogen 1s orbital is −13.6 eV. A better electron-donating ligand than "normal" hydrogen is characterized by H_{ii} higher than −13.6 eV and a poorer electron-donating ligand is characterized by H_{ii} lower than −13.6 eV. Ligands of variable electron-donating power were represented by varying the H_{ii} value of the four hydrogen atoms between −15.6 and −12.6 eV. The Natural Bond Orbital (NBO) charges and the Natural Resonance Theory (NRT) analysis were obtained using the NBO methodology with the NBO 5.0 program.[31]

RESULTS

In d^4 ML_4 species, where two d orbitals are used to host the four metal electrons, the $(n + 1)$s and three nd metal orbitals are available to form the four metal−ligand bonds. This leads to sd^3 hybridization at the metal, and the shape of the complex is determined by the optimal spatial distribution of these four sd^3 hybrids. The neutral polyhydride complex, d^4 MH_4, is an ideal system in that the H−M−H angles are very close to those that minimize the overlap between the metal hybrid orbitals at the metal which are 71° and 109°.[7a,8,32] It results that the structures can be constructed by placing the metal at a center of a cube and the four ligands at four vertices such that no ligands are trans (Figure 1). This gives three possible structures, which

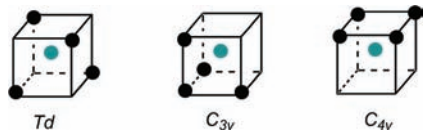

Figure 1. Dispositions of ligands for sd^3 hybridization in idealized d^4 ML_4 (M in blue at the center of the cube and L in black).[8]

have the shape of a tetrahedron, **td**, an umbrella, **umb**, and a 4-legged-piano stool, **pst**, as shown in the top part of Figure 2. In **td**, all coordination sites are equivalent and all bond angles are 109°. In **umb**, there are three basal hydrides, H_b, and one apical hydride, H_a, with H_a−M−H_b and H_b−M−H_b angles of 71° and 109°, respectively. In **pst**, the four hydrides are equivalent, and the cis H−M−H angle is equal to 71°. Changing the metal and

dx.doi.org/10.1021/ic3001448 | Inorg. Chem. 2012, 51, 5705−5715

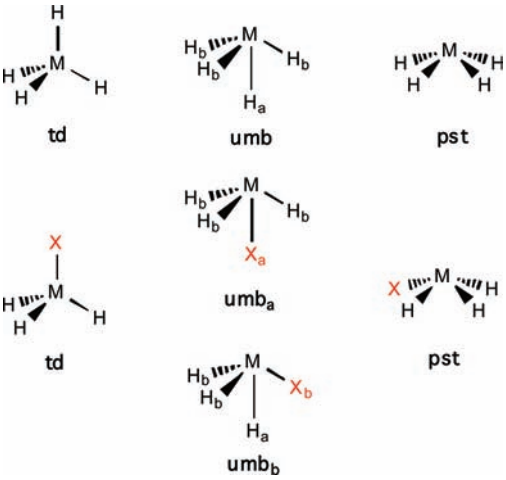

Figure 2. Possible structures for d^4 MH_4 (top) and d^4 MH_3X (bottom) with labeling.

the ligands lead to different angles, which influence the opening of the umbrella and the height of the piano stool.

When one of the three hydrogen atoms is replaced by an X ligand, tetrahedral, umbrella, and 4-legged piano stool isomeric structures are still found (Figure 2 bottom). Only the umbrella complex has nonequivalent sites. The presence of X gives rise to two isomers, namely, **umb$_a$** where X is at the apical site and **umb$_b$** where X is at the basal site.

Validation of the Use of Single Reference Methods for d^4 MH_3X. The geometries of MH_3X were optimized at a DFT level and the energetics were obtained with methods 2, 3, and 4, DFT (PBE0 and RSH+MP2), and CCSD(T), respectively. However, the use of single reference (SR) methods for the description of unsaturated species could be questionable. Even with truncation of excitations at the double and triple level, single reference methods, such as CCSD(T), recover a large portion of the dynamic correlation energy, but may fail when a significant amount of nondynamical correlation energy is present. In contrast, multireference methods, such as MRCI or MR-ACPF, recover both dynamical and nondynamical correlation energies.

To check the validity of the SR calculations for d^4 MH_3X, single points MRCI and MR-ACPF-2a calculations were carried out for the three isomers of RuH_4 (**td**, **umb**, and **pst**). For these MRCI and MR-ACPF-2a calculations, the reference space was built from full valence CASSCF orbitals (12 electrons, 10 orbitals) and the effect of the rejected configurations was estimated using second order perturbation theory (Table 1).

All calculations show that the **umb** and **pst** isomers are lower in energy than the **td** isomer. Furthermore, all methods give a similar energetic pattern. **Umb** and **pst** are lower than **td** by 9.1 to 12.9 and 9.4 to 14.7 kcal mol^{-1}, using the PBE0, RSH+MP2, and CCSD(T) methods, respectively. There is a marginal tendency for **pst** to have a lower energy than **umb**. It is also worth noting that the range separated hybrid RSH+MP2 calculations and the single reference coupled cluster calculations give values that are close. This overall good agreement between the single reference and multireference methods suggests that these unsaturated metal species do not contain a significant amount of nondynamical correlation energy. This indicates that a single reference method can be used for the computational study of d^4 MH_3X.

Table 1. Energetics[a] of RuH_4 Using the td Isomer as Reference

method	umb	pst
PBE0	−9.1	−9.4
RSH+MP2	−11.6	−12.3
CCSD(T)	−12.9	−14.0
MRCI	−10.6	−14.7
MR-ACPF-2a	−9.2	−13.7

[a]In kcal mol^{-1}.

In addition, several diagnostics have been suggested to evaluate the SR/MR character for molecular systems. The T_1 and D_1 diagnostics[33] (the Frobenius norm and matrix 2-norm of coupled cluster amplitudes for single excitations respectively) are arguably the most widely used diagnostics for SR coupled cluster calculations. Alternatively, the weight (C_0^2) of the leading configuration state function in a MRCI can be used to determine the multireference character. The T_1 and D_1 diagnostics were tested primarily on small organic molecules, and it was suggested that any T_1 diagnostic larger than 0.02 and any D_1 diagnostic larger than 0.05 invalidate the use of SR methods. However, a recent study of Jiang et al. pointed out that the criteria established for organic molecules ($T_1 < 0.02$ and $D_1 < 0.05$) are no longer valid for molecular systems with transition metals element.[34] On the basis of a statistical analysis of a set of 225 species, these authors proposed $T_1 < 0.05$ and $D_1 < 0.15$ as amplitude criteria for the validation of SR-based methods in the case of d-block energetics. The T_1 and D_1 diagnostics of the single reference CCSD(T) calculations are reported in Table 2 for the three isomers of RuH_4 (**td**, **umb**, and **pst**); the weight of the leading configuration (C_0^2) from the multireference MRCI or MR-ACPF-2a calculation is also indicated. For the three isomers of RuH_4, both T_1 and D_1 diagnostics from SR CCSD(T) calculations are less than the values suggested by Jiang et al. as acceptable limits. In addition, the weight of the leading configuration is higher than 0.80 for the MRCI and MR-ACPF-2a calculations. This confirms that these unsaturated molecular systems do not contain any substantial MR character. Single references methods are thus validated for the calculations of RuH_4. This validation applies to all d^4 MH_3X and MX_4 studied in this article (T_1 and D_1 diagnostics given in the Supporting Information for RuH_3X and OsH_3X).

Table 2. T_1 and D_1 Diagnostics of the Single Reference CCSD(T) Calculations and Weight of the Leading Configuration (C_0^2) of MRCI and MRACPF2 Calculations for the Three Isomers of RuH_4

	td	umb	pst
T_1	0.048	0.045	0.043
D_1	0.091	0.100	0.089
C_0^2 (MRCI)	0.82	0.84	0.84
C_0^2 (MRACPF2)	0.81	0.83	0.83

RuH_3X. *(a). RuH_4.* The DFT calculations show that RuH_4 has **td**, **umb**, and **pst** minima. The **umb** and **pst** isomers have similar energies and both species are more stable than the tetrahedral structure by about 9 kcal mol^{-1}. These results differ from those obtained by Landis. Molecular mechanic (MM) calculations including hybridization and resonance in a valence bond (VB) approach (Hypervalent-VALBOND (HV-VB) MM

dx.doi.org/10.1021/ic3001448 | Inorg. Chem. 2012, 51, 5705−5715

method)[9] give the same three minima but show that **td** is the most stable isomer. DFT calculations using a different ECP and a different functional for the metal[7a,9] from the one used in this work give **td** and **pst** as the only minima, with **pst** being 8.6 kcal mol^{-1} lower in energy relative to **td**. The Hartree−Fock and MP2 calculations by Hall et al. show several isomers with relative energies that depend on the computational method used.[10]

The essential structural features of the three isomers of RuH_4 are shown in Figure 3. The Ru−H bond is 1.55 Å in **td**. In **umb**,

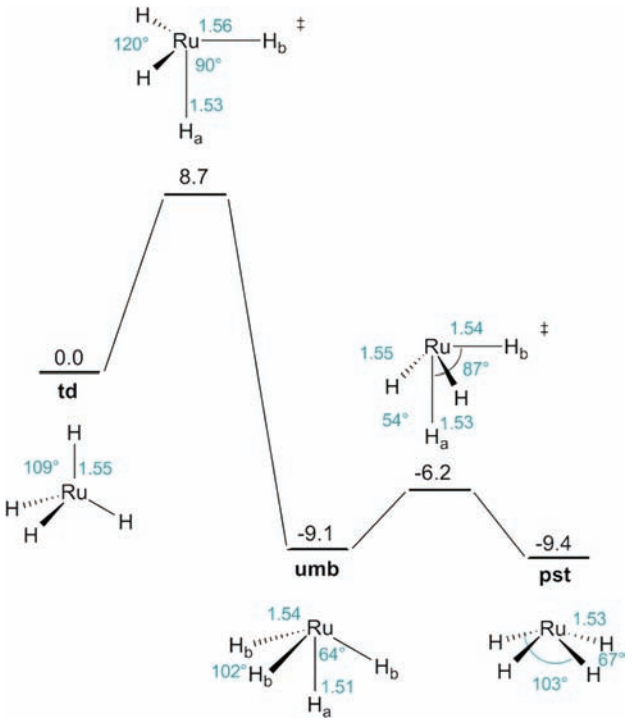

Figure 3. DFT optimized structures of minima and transition states of interconversion between minima for RuH_4. The distances are in Å and the angles in degrees. The DFT energies are given in kcal mol^{-1} relative to the **td** structure, using method 2.

the apical Ru−H_a bond of 1.51 Å is slightly shorter than the basal Ru−H_b bond of 1.54 Å. The H_b−Ru−H_a and the H_b−Ru−H_b angles of 64° and 102°, respectively, are close to the corresponding ideal values of 71° and 109° predicted for a sd^3 hybridized metal. The acute H_b−Ru−H_a angle leads to a nonbonded $H_a\cdots H_b$ distance of 1.62 Å, which is less than the sum of the van der Waals (vdW) radii of the two hydrogens (1.20 Å).[35] In **pst**, the Ru−H bond of 1.53 Å and the angles of 67° and 103° for cis H−Ru−H and trans H−Ru−H angles, respectively, are similar to the ideal values of 71° and 109°. In **pst**, the shorter nonbonded H···H distance is 1.69 Å, which is less than the sum of the vdW radii of the two hydrogens although slightly longer than in **umb**. Therefore, both **umb** and **pst** have short nonbonded H···H distances that are not present in the **td** structure wherein the H···H nonbonded distance is 2.54 Å.

The transition states between these minima were searched using method 2 to evaluate the depth of the associated wells on the potential energy surface and the possibility of exchange between the three minima (Figure 3). A transition state of 8.7 kcal mol^{-1} above **td** was located between **td** and **umb** and another transition state between **umb** and **pst** with an energy of 2.9 kcal mol^{-1} above **umb**. No transition state was identified between **td** and **pst**. The tetrahedral structure is thus separated from the other minima by a significant barrier, but there is a low energy barrier between **umb** and **pst**. The structural features of the two transition states are shown in Figure 3. The transition state between **td** and **umb** isomers inverts the configuration at the metal as it inverts the umbrella. At the transition state, the ruthenium atom is in the equatorial plane formed by the three H_b hydrogens and the Ru−H_a bond is perpendicular to the equatorial plane; this inversion at the metal occurs without significant change in the Ru−H bond distances. The transformation of **umb** to **pst** is a concerted swinging motion of two H_b relative to the plane defined by Ru−H_a and the third Ru−H_b bonds. At the transition state, Ru−H_a and two Ru−H bonds are coplanar. This transformation also occurs without significant change of the Ru−H bond distances.

(b). RuH_3X (X = H, F, CH_3, CF_3, SiH_3, and SiF_3). The structures of RuH_3X (X = H, F, CH_3, CF_3, SiH_3, and SiF_3) were determined at the DFT level with method 2. The results are shown in Figure 4 as a histogram in which the energies of the

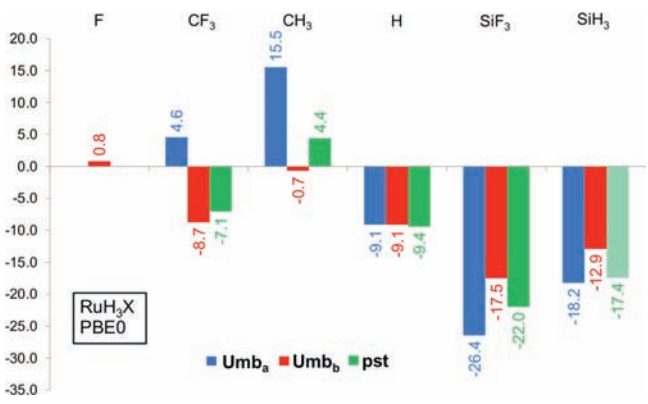

Figure 4. DFT energies, in kcal mol^{-1}, for RuH_3X (X = F, CF_3, CH_3, H, SiF_3, and SiH_3) complexes, relative to the tetrahedral isomer, **td**. The energies are in blue for the umbrella with apical X, $\mathbf{umb_a}$ in red for the umbrella with basal X, $\mathbf{umb_b}$, and in green for the 4-legged piano-stool structure, **pst**. Light green is used to indicate structures with hydride bridging Ru−Si.

non-tetrahedral structures are plotted relative to the **td** structure, which is a minimum for all X groups. Figure 4 shows that X influences the relative energies of the various minima and also the number of minima. For instance, RuH_3F has only two minima, **td** and $\mathbf{umb_b}$, while the four minima shown in Figure 2 are obtained for all other X.

Single point calculations with method 3, RSH+MP2, and method 4, CCSD(T), are shown in Figure 5. These calculations show energetic patterns similar to that obtained with method 2. Methods 3 and 4 stabilize more the non-tetrahedral structures relative to the tetrahedral references than method 2. In the case where method 2 gives a non-tetrahedral structure less stable than **td**, the difference in energy between **td** and non-tetrahedral structures is decreased. In the case where method 2 gives a non-tetrahedral structure more stable than **td**, the difference in energy is increased.

In RuH_3F, the isomers **td** and $\mathbf{umb_b}$ are isoenergetic. The Ru−H bond lengths and the angles between the Ru−H bonds are similar to that of RuH_4 in the corresponding isomers. The Ru−F is longer at the basal site of $\mathbf{umb_b}$ than in **td** (1.85 and 1.80 Å, respectively). The F−Ru−H_a angle is nearly 92° in

dx.doi.org/10.1021/ic3001448 | Inorg. Chem. 2012, 51, 5705−5715

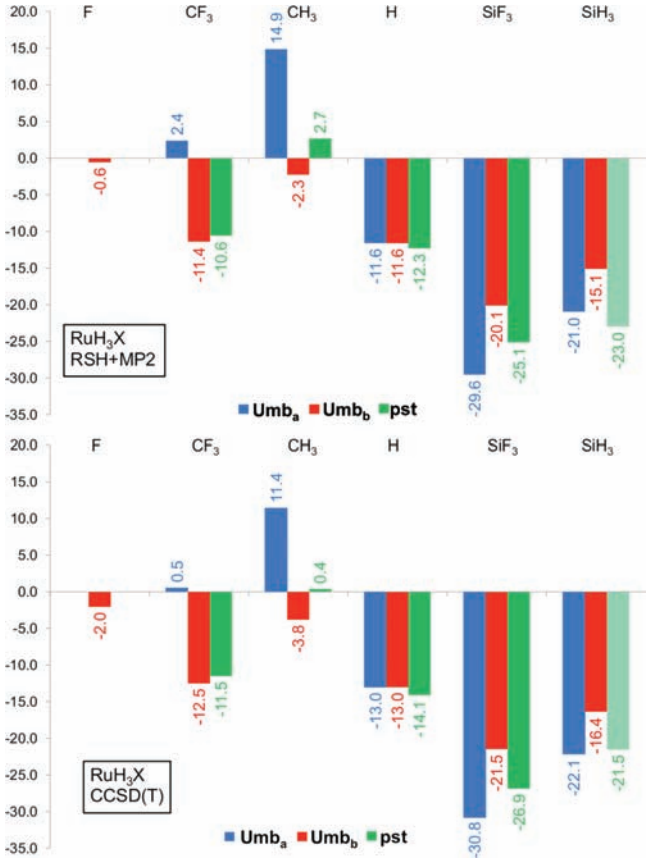

Figure 5. RSH+MP2 (top) and CCSD(T) (bottom) energies, in kcal mol^{-1}, for RuH_3X (X = F, CF_3, CH_3, H, SiF_3, and SiH_3) complexes, relative to the tetrahedral isomer, **td**. The energies are in blue for the umbrella with apical X, **umb**$_a$, in red for the umbrella with basal X, **umb**$_b$, and in green for the 4-legged piano-stool structure, **pst**.

umb$_b$, which is notably different from the H_b-Ru-H_a angle of 63°. For RuH_3CH_3, the **td**, **umb**$_b$, and **pst** have similar energies and **umb**$_a$ is significantly higher in energy. Although the four minima have shapes that are overall similar to the corresponding minima of RuH_4, some structural aspects need to be mentioned. The Ru−C bond length of 1.95 Å in **td** is slightly shorter than in the other isomers (1.96 to 2.1 Å). In **umb**$_b$, the methyl group moves away from the axis of the umbrella as indicated by the CH_3-Ru-H_a angle of 80°, which is larger than the H_b-Ru-H_a angle of 66°. Likewise, in **pst**, the CH_3-Ru-H angle of 81° is larger than that of 63° between two cis Ru−H bonds. RuH_3CF_3 also has four minima, the most stable ones being **umb**$_b$ and **pst** by about 8 kcal mol^{-1} at the DFT level. The structural features of the RuH_3CF_3 and RuH_3CH_3 complexes are similar.

RuH_3SiH_3 and RuH_3SiF_3 also have the four minima like were found for RuH_3CH_3 and RuH_3CF_3. However, the energy pattern for the alkyl and the silyl ligands is significantly different. For the silyl ligand, all non-tetrahedral structures are at significantly lower energy than the tetrahedral structure by about 18 kcal mol^{-1} at the DFT level. In addition, the influence on the geometries is also different for the silyl and the methyl ligands. For instance, in the **umb**$_a$ isomer of RuH_3SiH_3, the Ru−Si distance of 2.26 Å is slightly shorter than in **td**, 2.30 Å, and the Si−Ru−H angles are similar to the corresponding H−Ru−H angles. In **umb**$_b$ of RuH_3SiH_3 the $Si-Ru-H_a$ angle is equal to the H_b-Ru-H_a angle. Thus, the Si−Ru−H angles are systematically smaller than the corresponding C−Ru−H angles in the non-tetrahedral geometry. For the **pst** structure, one of the hydrogen of the SiH_3 group bridges the Ru−Si bond. The ability for the silyl group and notably the SiH_3 group to enter in the bridging situation is well documented and is not the focus of this study.[36]

As a partial summary, these calculations show that all RuH_3X have several isomeric structures, among which the tetrahedral structure is not always the most stable isomer. For X = F and CH_3, the **td** structures are isoenergetic with the other isomers. In the case of X = H, CF_3, SiH_3, and SiF_3, there is a clear preference for non-tetrahedral structures especially with the silyl ligands. The structures of the **td**, **umb**$_a$, **umb**$_b$, **pst** isomers are rather similar for all X and, thus, the structure of RuH_4 is a good representative of the entire set. There is a noticeable tendency for the X groups that favor significantly the non-tetrahedral structures (SiH_3 and SiF_3) to have a structure close to that of RuH_4. In contrast, for the X groups that do not favor the non-tetrahedral structures (F and CH_3), the X−Ru−H angle is systematically larger than the corresponding H−Ru−H angle. This structural pattern will reveal through-space interaction in the non-tetrahedral structures, as it will be discussed later.

For all systems, the various non-tetrahedral structures are separated by low energy barriers and therefore non-tetrahedral structures are fluxional. However, the non-tetrahedral structures are separated from the **td** structure by a barrier that is significantly higher than their difference in energy with the exception of RuH_3SiF_3 where the energy barrier is very close to the difference in energy. See Supporting Information for further details.

OsH_3X (X = H, F, CH_3, CF_3, SiH_3, and SiF_3). Three minima were located for OsH_4 (Figure 6). In contrast to the preference for non-tetrahedral structures found for RuH_4, the three isomers of OsH_4 are isoenergetic. Similar results have been obtained by Landis et al. with **umb** and **pst** being 3.5 and 5.2 kcal mol^{-1} above the **td**.[37] The structures of **td**, **umb**, and **pst** are similar to those found for RuH_4. An energy barrier of 10.9 kcal mol^{-1} relative to **td** separates **td** and **umb**,[37] and an energy barrier of 5.8 kcal mol^{-1} relative to **umb** separates **umb** and **pst**.

The DFT energies for OsH_3X (X = F, CF_3, CH_3, H, SiF_3, and SiH_3), relative to the **td** isomers, are shown as a histogram in Figure 7 using the convention already used in Figure 4 for RuH_3X. There is a significant difference between the isoelectronic ruthenium and osmium complexes. For X = F, CH_3, and CF_3, the tetrahedral structure is more stable than any non-tetrahedral isomer. For X = H, the tetrahedral and non-tetrahedral isomers have similar energies. For X = SiH_3 and SiF_3, the preference for the non-tetrahedral structure remains, but the difference in energy between **td** and non-tetrahedral structures decreases by about 10 kcal mol^{-1}, compared to the ruthenium complexes. Thus, everything being equal, replacing ruthenium by osmium increases the stability of the tetrahedral isomer relative to the non-tetrahedral.

$[ReH_3X]^-$, $[RhH_3X]^+$, and $[IrH_3X]^+$. To further understanding of the effect of the metal on the structural preference of d^4 MH_4, the isoelectronic anionic $[ReH_3X]^-$ and cationic $[RhH_3X]^+$, $[IrH_3X]^+$ species were optimized with method 2, and single points RSH+MP2 energies were obtained with method 3.

$[ReH_4]^-$ and $[IrH_4]^+$ have three minima while $[RhH_4]^+$ has two minima, Figure 8. The anionic $[ReH_4]^-$ has a preference for the tetrahedral structure while the cationic $[RhH_4]^+$ and

dx.doi.org/10.1021/ic3001448 | Inorg. Chem. 2012, 51, 5705−5715

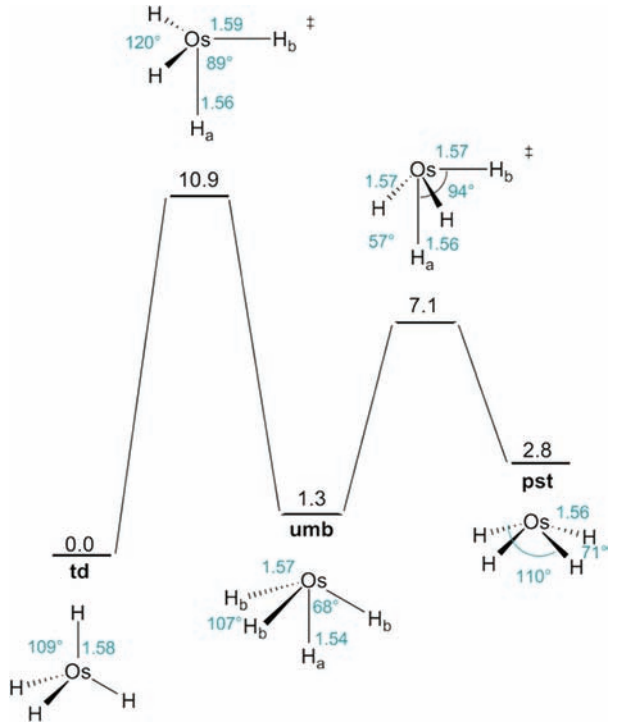

Figure 6. DFT optimized structures of minima and transition states of interconversion between the minima for OsH_4. The distances are in Å and the angles in degrees. The energies are given in kcal mol^{-1} relative to the **td** structure, using method 2.

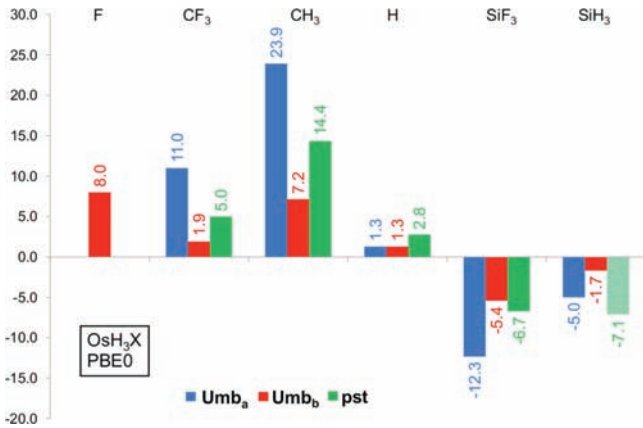

Figure 7. DFT energies, in kcal mol^{-1}, for OsH_3X (X = F, CF_3, CH_3, H, SiF_3, and SiH_3) complexes, relative to the tetrahedral structure, **td**, with similar conventions as in Figure 4.

$[IrH_4]^+$ have a preference for non-tetrahedral geometries. The preference for the non-tetrahedral relative to the tetrahedral structures is stronger for the cationic than for the neutral species; for $[RhH_4]^+$ the preference for non-tetrahedral structure increases by over 25 kcal mol^{-1} relative to RuH_4. For $[IrH_4]^+$, the preference for the non-tetrahedral structure is more marked than for OsH_4 but less so than for RhH_4^+. The influence of the total charge and the nature of metal on the preferential structures of d^4 $[MH_4]^q$ (q = −1, 0, and 1) is thus important. Consequently, going from the left to the right of the periodic table increases the preference for non-tetrahedral geometries but going down a column decreases this preference.

The geometries of the minima for $[ReH_4]^-$, and $[IrH_4]^+$ are similar to those previously found for RuH_4. The H−M−H

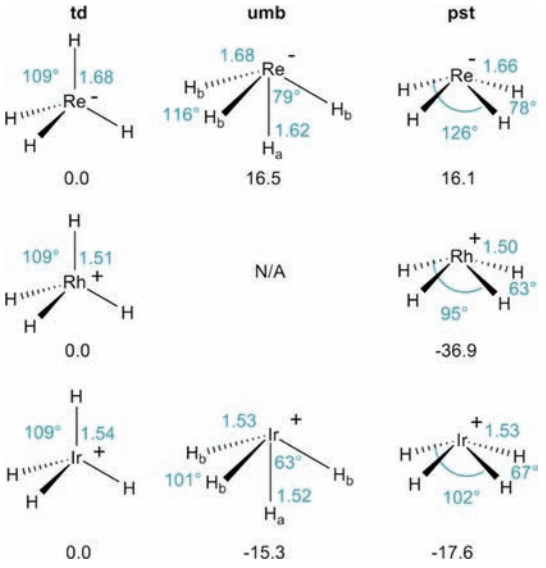

Figure 8. DFT optimized geometries (distances are given in Å and angles in degrees) of $[ReH_4]^-$, $[RhH_4]^+$, and $[IrH_4]^+$. The energies are given in kcal mol^{-1} relative to **td**. N/A signifies that no minimum of this type could be located.

angle shows a pattern that parallels the preference for the non-tetrahedral structures. In the **umb** isomer of $[ReH_4]^-$, the H_a−M−H_b and the H_b−M−H_b angles are larger than in the neutral systems. A similar pattern is seen in the **pst** isomer. The opposite trend is found in the cationic systems. For $[IrH_4]^+$, the minima are those of the type shown in Figure 2. In the case of $[RhH_4]^+$, the **pst** isomer is a highly fluxional structure where the decrease of a cis H−Rh−H angle from 63 to 38° occurs with essentially no energy cost. No **umb** type structure was located as minimum. Overall, the structures of isoelectronic d^4 MH_4 are thus sensitive to the total charge; a negative charge opens the umbrella and flattens the 4-legged piano stool and a positive charge closes the umbrella and raises the height of the 4-legged piano stool. Going down a column of the periodic table also opens the umbrella and flattens the 4-legged piano stool.

The histograms for the relative energies of the isomers for $[ReH_3X]^-$, $[RhH_3X]^+$, and $[IrH_3X]^+$ are shown in the Supporting Information. The pattern of energies can be understood from the pattern obtained for the ruthenium and osmium complexes. For $[ReH_3X]^-$ (X = F, CF_3, CH_3, H, SiH_3, and SiF_3) the preference for the tetrahedral structure decreases from CH_3 to SiF_3. However, the combined effect of the negative charge and the 5d metal results in a general preference for the tetrahedral coordination for any X; in the case of $[ReH_3F]^-$ the tetrahedral structure is the only minimum. For X = CH_3, CF_3, and SiH_3, the tetrahedral structures are more stable than the non-tetrahedral structures, and, in the case of $[ReH_3SiF_3]^-$, **pst** and **td** are isoenergetic. For $[IrH_3X]^+$ the preference for non-tetrahedral structures is found for X = SiF_3 and SiH_3. For X = CH_3 and CF_3, non-tetrahedral structures are preferred except for the **umb** structure with apical X group that is significantly less stable than **td**. In the case of $[IrH_3F]^+$, the $\mathbf{umb}_b$ structure with equatorial F is marginally more stable than **td**, but the $\mathbf{umb}_a$ structure with apical F is significantly less stable than **td**. In the case of $[RhH_3X]^+$, non-tetrahedral structures are more stable than **td** for X = H, SiF_3 and SiH_3. For X = CF_3 and CH_3, structures of different natures than found for

dx.doi.org/10.1021/ic3001448 | Inorg. Chem. 2012, 51, 5705−5715

all other metal complexes are found to be more stable than tetrahedral structure. No comparison can be done with the other cases, and this was not explored further.

RuX_4. The diamagnetic homoleptic $Ru(C_6H_{11})_4$,[11] Ru(o-Tolyl)$_4$,[12] Ru(Mesityl)$_4$,[13] $Os(C_6H_{11})_4$,[11] Os(o-Tolyl)$_4$,[14] and Ir(Mesityl)$_4^+$,[13] which are the only 12-electron d^4 MR_4 complexes to have been synthesized and fully characterized, are remarkably stable. They are colored as expected from the presence of low-lying empty metal d orbitals. In all cases, X-ray diffraction studies show that these complexes have a tetrahedral structure in the solid state. The NMR study of the tetramesityl complex of ruthenium shows a fluxional behavior attributed to the rotation of the ligand about the Ru−C bond.[13] To better compare with the experimental structures, RuX_4 complexes were calculated for X = F, CH_3, CF_3, SiH_3, and SiF_3. The optimization of RuF_4 and $Ru(CF_3)_4$ yields only tetrahedral isomers. Two minima are found for $Ru(CH_3)_4$ with the **td** structure being 32.2 kcal mol^{-1} below the **pst** structure. A preference for non-tetrahedral isomers is obtained with the silyl substituted complexes. For $Ru(SiH_3)_4$ and $Ru(SiF_3)_4$, the **umb** isomer is 12.6 kcal mol^{-1} and 17.1 kcal mol^{-1} more stable than the **td** isomer, respectively. In addition, structures with a **pst** shape in which the SiH_3 and SiF_3 ligands have hydrides or fluoride bridging the Ru−Si bond are also located as minima lower than the **td** isomer (−29.8 and −23.5 kcal mol^{-1} for $Ru(SiH_3)_4$ and $Ru(SiF_3)_4$, respectively), but they will not be considered. These calculations on homoleptic complexes show that non-tetrahedral geometries are possible even with ligands more bulky than H. Furthermore, the energy trend obtained for RuH_3X (Figure 4) is also present for RuX_4. Fluorine is the ligand that most disfavors the non-tetrahedral geometry in the RuH_3X series; consequently RuF_4 has only a tetrahedral structure. The CH_3 ligand disfavors slightly less the non-tetrahedral structures; consequently a non-tetrahedral structure is found as a high-lying secondary minimum. Finally, SiH_3 and SiF_3 ligands, which most favor non-tetrahedral structures in the RuH_3X series, lead to homoleptic complexes with preference for non-tetrahedral structures. The only exception to this trend is the case of $Ru(CF_3)_4$ whose tetrahedral structure cannot be predicted from the influence of a single CF_3 ligand on the structural preference of $RuH_3(CF_3)$. Clearly, the structures of the alkyl and aryl complexes that have been synthesized do not display the diversity of possible structures for d^4 RuX_4.

DISCUSSION

The bonding analysis of Landis and Weinhold[8] as well as the ORSAM analysis of Hall[10] show that d^4 MH_3X and MX_4 have several structures. In this analysis, the metal uses the $(n + 1)$s and the nd orbitals, which are not occupied by the electrons of the metal lone pairs to establish the covalent metal−ligand bond. For an sd^3 hybridization that applies to d^4 tetracoordinated complexes, the tetrahedral structure is one of the possible structures. The non-tetrahedral structures have umbrella and 4-legged piano stool shapes. However, the valence-bond analysis of Landis and Weinhold[8] and the ORSAM model of Hall[10] do not provide any information on the relative energies of the various isomeric forms. The DFT and ab initio calculations show that the metal and the ligands influence significantly the relative energies of the several isomers. In MH_3X, the non-tetrahedral structures have nonbonded distances between proximate atoms that are relatively short. This is the case in particular for MH_4 wherein the nonbonding H···H distances in the non-tetrahedral geometries are shorter than the sum of the vdW distances. The increased steric hindrance resulting from the replacement of the hydrogens in RuH_4 by relatively bulky alkyls and aryl ligands could have been the reason for all experimentally known systems to be tetrahedral. However, the calculations show that CH_3 and SiH_3 ligands lead to opposite structural preference, the former ligand increasing the preference for the tetrahedral structure and the latter for the non-tetrahedral structures. These trends apply to RuH_3X and RuX_4 showing that the steric effects of groups larger than hydrides do not determine the structural preferences. Calculations show that the metal also plays an important role on the structural preference. Going from the left to the right of the periodic table, that is, from anionic to cationic isoelectronic complexes increases the preference for the non-tetrahedral structures while going down a column of the periodic table increases the preference for the tetrahedral structures. Factors that also play a role are, among others, the relative electronegativity of the metal and the electron-donating/electron-withdrawing ability of the ligands. To understand better these factors, a molecular orbital analysis, based on EHT calculations, has been carried out for RuH_4 and a NBO charge analysis complemented by a NRT analysis based on the calculated DFT densities have been carried out for RuH_4 and OsH_4.

(a). Molecular Orbital Analysis. The EHT total energies of the **td**, **umb**, and **pst** structures for RuH_4 give a preference for a non-tetrahedral structure. Increasing the electron-withdrawing ability of the ligand by lowering the hydrogen H_{ii} Coulombic integral gives a preference for a tetrahedral structure. This modeling of ligands reproduces the results of the DFT calculations. For instance (i) F and CH_3 are more electron-withdrawing than H and SiH_3 and thus favor the tetrahedral structure, (ii) Os 5d orbitals are higher in energy than Ru 4d orbitals and thus ligands appear to be more electron-withdrawing relative to Os than Ru. Likewise, in a cationic complex where the metal is more electron-attracting, all ligands appear more electron-donating. The reverse is true for anionic complexes.

A Walsh diagram is used to gain further insight into why EHT calculations reproduce qualitatively the structural preference obtained with higher-level calculations. Only the occupied molecular orbitals of RuH_4 are necessary in this analysis (Figure 9). The C_{3v} or C_{4v} group notations are used for labeling the molecular orbitals for the three structural forms. The **td** structure has two nonbonding d orbitals of e symmetry to host four electrons. The four Ru−H bonds are represented by two molecular orbitals of a_1 symmetry and two orbitals of e symmetry. Only the molecular orbitals of a_1 symmetry have a contribution on the hydrogen located on the z axis. In **umb**, all molecular orbitals of e symmetry have the same energy as in **td** because they have no contribution on the hydrogen on the z axis. The only molecular orbitals, which have different energies for **td** and **umb**, are the molecular orbitals of a_1 symmetry. They are constructed in a similar manner in **td** and **umb**. The lower one, $\mathbf{1a_1}$, is the in-phase combination of the metal 5s orbital and the 1s orbital of the four hydrogens. The higher orbital of a_1 symmetry, $\mathbf{2a_1}$, is mostly made of the in-phase combination of a d_{z^2} with the four hydrogens. The contribution of the 5p orbitals has been found to be negligible in all molecular orbitals even if permitted by symmetry; it will not be mentioned further. The key point of the analysis is that, in $\mathbf{2a_1}$, the coefficient of the hydrogen on the z axis has the sign opposite to that of the three other hydrogens, which are in-phase with the torus part of d_{z^2}.

dx.doi.org/10.1021/ic3001448 | Inorg. Chem. 2012, 51, 5705−5715

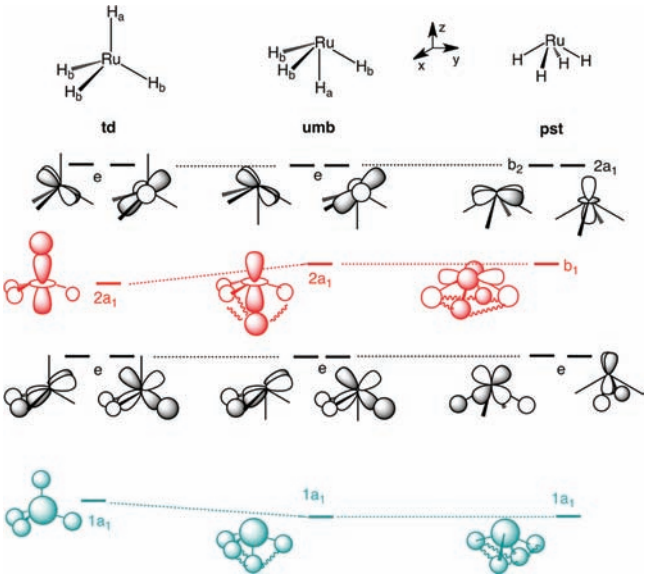

Figure 9. Walsh diagram for the **td** to **umb** and **pst** transformation. The green orbitals are stabilized from **td** to either **umb** or **pst** and the red orbitals are destabilized. The green and red wriggling lines indicate positive and negative overlaps, respectively.

The energy of $\mathbf{1a_1}$ is thus lower in **umb** than in **td** because the in-phase relationship between all hydrogens stabilizes the orbital when the hydrogen atoms are closer (**umb** vs **td**). In contrast, the energy of $\mathbf{2a_1}$ is higher in **umb** than in **td** because the out-of-phase relationship between the apical and basal hydrogens raises the energy of this molecular orbital when the distances between the nonbonded hydrogens are shorter and the overlap increases. Two antagonist effects are thus at work and **umb** is more stable than **td** if the energy lowering of $\mathbf{1a_1}$ is more important than the energy rise of $\mathbf{2a_1}$. The $\mathbf{1a_1}$ orbital is more located on the hydrogens than on the metal because the energy level H_{ii} of the hydrogen 1s orbital is always lower than the energy value H_{ii} of the 5s of the metal. In contrast, the $\mathbf{2a_1}$ orbital is more located on the metal when the energy of the hydrogen 1s orbital is higher than that of the metal d orbital, and it is more located on the hydrogen atoms when it is lower. Therefore, the energy rise of the $\mathbf{2a_1}$ orbital upon going from **td** to **umb** is small in the first case and large in the second case. Consequently, electron-donating ligands favor **umb** and electron-withdrawing ligands favor **td**.

A similar reasoning applies to the comparison between **td** and **pst**. In **pst**, the four nonbonding metal electrons are hosted in $\mathbf{2a_1}$ (d_{z^2}) and $\mathbf{b_2}$ (d_{xy}) orbitals (Figure 9). The four Ru−H bonding orbitals are described by an $\mathbf{1a_1}$ orbital made mostly from the metal s orbital, two orbitals of e symmetry made mostly from the metal d_{xz} and d_{yz} orbitals, and a $\mathbf{b_1}$ orbital made from $d_{x^2-y^2}$. The contribution of the 5p orbitals has been found to be negligible even if permitted by symmetry, as already noted above. The $\mathbf{1a_1}$ orbital favors the **pst** structure because of the in-phase relationship between all hydrogens. The $\mathbf{b_1}$ orbital disfavors the **pst** structure because of the out-of-phase relationship between the hydrogens. The two degenerate orbitals of e symmetry have essentially no influence on the structural preference because of the long distance between the two trans hydrogens. The influence of the energy level H_{ii} of the hydrogens on the variation of energy of the $\mathbf{1a_1}$ and $\mathbf{b_1}$ orbitals between **td** and **pst** is similar to that obtained for the case of **td** vs **umb**. Electron-donating ligands favor **pst** and electron-withdrawing ligands favor **td**.

(b). NBO Charge Analysis. The NBO charges for RuH_4 and OsH_4 are shown in Figure 10. For these two species in which the metal is formally at a high oxidation state, M^{IV}, the NBO charge at the metal is negative indicating, as currently recognized, that the calculated charge has no relation with formal oxidation state. The negative charge is small for the **td** complexes but increases to a maximum value of −0.3 for the non-tetrahedral species. Accordingly, the charge on the hydrogens is very small and positive in RuH_4. In the non-tetrahedral structures, the hydrogens carry a positive charge; the largest positive charge is carried by the apical hydrogen of **umb**. The results are qualitatively similar for OsH_4, but the electronic density on the metal is smaller for Os than for Ru and the charge is even marginally positively charge in **td**. The charge distribution in the Ru and Os complexes does not give a rationale for the stronger energetic preference for non-tetrahedral structures in the case of Ru. However, the charge distribution indicates that electron-donor ligands are beneficial for the non-tetrahedral structures.

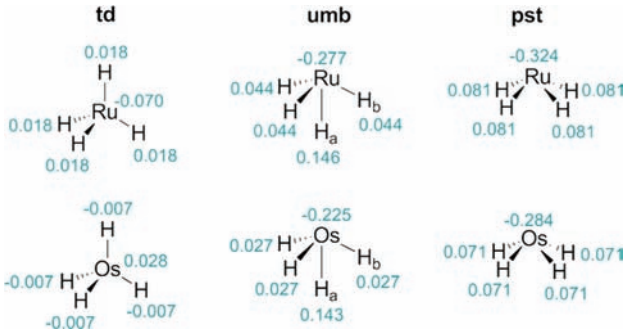

Figure 10. NBO charges in RuH_4 and OsH_4.

(c). NRT Analysis. A natural resonance (NRT) analysis[38] of the DFT density was carried out for the three isomers, **td**, **umb**, and **pst** of RuH_4 and OsH_4. This analysis is aimed at determining the valence structures that describe the total electron density of these complexes in the various isomeric forms.[8] This analysis has met some criticism[38a] but has been found to be qualitatively useful for understanding electronic structures.[8] The results are shown in Figure 11. In the **td** isomer, the dominant structure has four covalent M−H bonds and two lone pairs at the metal. This valence structure accounts for 97% of the density for RuH_4 and 98% for OsH_4. For the **umb** isomer, the same structure accounts for only 80% of the total density for RuH_4 and 90% for OsH_4.[39] The remaining part of the electron density is represented by structures with two covalent M−H bonds, three lone pairs at the metal, and a proton and a hydride characterizing an ionic interaction between the metal fragment and the hydrogen atoms. The structure with a proton at the apical site has higher weight (12% for RuH_4 and 6% for OsH_4) than that with a hydride at the apical site (7% for RuH_4 and 3% for OsH_4). The structure with the proton and the hydride at the basal sites has the smallest weight 1%. For the **pst** isomer, the main structure is that with four M−H bonds and two lone pairs at the metal (79% of the total electron density for RuH_4 and 89% for OsH_4). The remaining part of the electron density is represented by a valence structure with two covalent M−H bonds, three lone pairs at the metal, and a proton and a hydride on cis hydrogen

dx.doi.org/10.1021/ic3001448 | Inorg. Chem. 2012, 51, 5705−5715

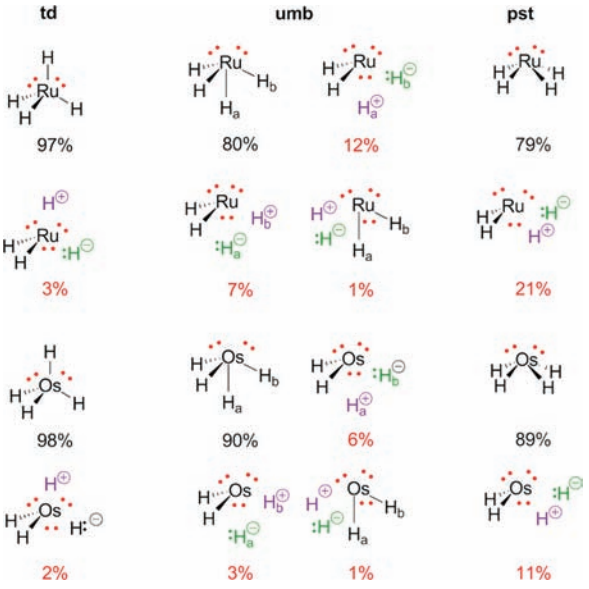

Figure 11. Main valence bond structures for RuH_4 and OsH_4. The value indicated below each structure represents the percentage of this structure that contributes to the total density. The values indicated are summed over all equivalent sites.

sites. It accounts for 21% of the density for RuH_4 and 11% of the density for OsH_4.

The total electron density is well described by these valence structures for all isomers of RuH_4 and OsH_4 since the sum of the contributions is 100%. In the valence structures displaying the ionic contributions, the proton and the hydride interact with the metal and also together since the two species with opposite charges are on atoms that are at relatively short distances. This gives rise to an electrostatic interaction that contributes to the stability of the **umb** and **pst** isomers. The structures with these ionic components have a higher weight for RuH_4 than for OsH_4, which could rationalize the preference for the **umb** and **pst** isomers in the case of RuH_4. The same analysis was carried out for RuH_3X (X = F, CH_3, and SiH_3) (see Supporting Information). In all cases, the tetrahedral structure is described by essentially a single structure with three M−H bonds, one M−X bond, and two lone pairs on the metal. The electron densities of **umb** and **pst** isomers are still dominated by the same valence structures but structures with two covalent bonds to the ruthenium, three lone pairs on the metal, and a positively charged group (H or X) and a negatively charged group (H or X) have relatively high percentages. It has not been possible to establish a quantitative correlation between the percentage of the valence structures with zwitterionic contributions and the relative energies of the non-tetrahedral and tetrahedral structures. However, it is likely that they play a key role in stabilizing the non-tetrahedral structures.

(d). Through-Space Interactions in the non-tetrahedral Structures from MO and NRT Analyses. The Walsh diagram and the NRT analyses provide a consistent interpretation of the stability of the non-tetrahedral structures of d^4 RuH_4 although they use different languages and properties of the electronic structures. In the molecular orbital analysis, it was shown that the out-of-phase contribution between nearby "hydrogen" orbitals, which disfavors the **umb** and **pst** isomers relative to the **td** isomers, depends on the electron-donating power of the "hydrogen" ligands to the metal center. Ligands that are good electron donor contribute less to this orbital than ligands that are less good electron donor. When this destabilizing interaction is low, the through-space stabilizing interaction arising from the all in-phase low-lying occupied orbital dominates. Structures with the shortest distances between nonbonded atoms, that is, **umb** and **pst**, are favored relative to **td**. These stabilizing interactions do not create any covalent bonds between these hydrogens but favor interatomic distances shorter than the sum of the vdW radii. The NRT analysis gives a complementary interpretation of the results. It confirms the absence of covalent bond between hydrogens that are at distance shorter than the sum of the vdW radii (axial H_a and basal H_b in **umb** and two cis basal H in **pst**). However, the NRT establishes the presence of an electrostatic interaction between positively and negatively charged hydrogens.

The analysis established for tetrahydride complexes can readily be generalized to complexes with any type of ligand. It provides an interpretation of the effect of the ligand using only the electron-withdrawing/electron-donating property of the ligands, but other factors can also contribute. For instance, fluorine is an electron-withdrawing ligand and thus the non-tetrahedral structures are disfavored. This result is suggested independently from the presence of the lone pairs on the fluorine lone pairs that would disfavor the presence of any group at short distance from fluorine as in the non-tetrahedral structures. Likewise, an alkyl group is reasonably electron-withdrawing and thus disfavors a non-tetrahedral structure. Steric effects between the alkyl group and the other ligands also disfavor the non-tetrahedral structures. At the other extreme, a good electron-donating group like a silyl group favors non-tetrahedral structures. In the case of a complex like $RuH_3(SiH_3)$ the stabilizing interactions that have been described above are supplemented by the well-known through space interaction between a hydride and a nearby silyl group, originating from the ability of silicon to become hypervalent. This interaction, which has been known as SISHA[40] or IHI,[41] is magnified when the silyl group is substituted by halide. This accounts for the preference for non-tetrahedral structures for $RuH_3(SiH_3)$ and $RuH_3(SiF_3)$. The fact that $Ru(SiH_3)_4$ and $Ru(SiF_3)_4$ also prefer non-tetrahedral structures show that interactions different from SISHA and IHI are at work.

■ CONCLUSIONS

DFT (PBE0 and range separated DFT, RSH+MP2) and CCSD(T) calculations have been used to determine the preferred structures of MH_3X^q (M = Ru, Os, Rh^+, Ir^+, and Re^-; X = H, F, CH_3, CF_3, SiH_3, and SiF_3) and MX_4 (M = Ru; X = H, F, CH_3, CF_3, SiH_3, and SiF_3). Tetrahedral and non-tetrahedral structures are found as possible minima. The non-tetrahedral structures (umbrella and 4-legged piano stool shaped complexes) are those predicted for an sd^3 hybridization following the analysis of valence bond of Landis et al. and the ORSAM analysis of Hall et al. The calculations show that non-tetrahedral structures can be energetically preferred to the expected tetrahedral geometry for certain metals and ligands. The non-tetrahedral isomers are more energetically preferred for 4d metal than for for 5d metals. Cationic complexes also tend to favor the non-tetrahedral isomers while anionic complexes do not. The relative energies of the non-tetrahedral and the tetrahedral structures are significantly influenced by the nature of the ligands. Electron-withdrawing ligands like halide and alkyl favor the conventional tetrahedral structure while ligands that are more electron donating like hydride and silyl

dx.doi.org/10.1021/ic3001448 | Inorg. Chem. 2012, 51, 5705−5715

favor the non-tetrahedral structures. The factors that determine these energy patterns have been discussed by means of a molecular orbital analysis based on EHT calculations and NBO charge analysis supplemented by an NRT analysis. All analyses show that electron-donating ligands favor the non-tetrahedral structures. Furthermore, the EHT and the NRT analyses suggest the presence of possible weak attractive interactions between atoms that are closer in **umb** and **pst** than in **td**. These weak attractive interactions are magnified when the ligands are good electron donor to the metal center.

■ ASSOCIATED CONTENT

Supporting Information

List of coordinates of all calculated structures with energies E and ZPE corrected energies (E + ZPE). Histograms of energies (methods 2 and 3) for $[ReH_3X]^-$, $[RhH_3X]^+$, and $[IrH_3X]^+$. Potential energy surfaces for the transformations between the various isomers of RuH_3X. NBO charges and NRT analysis for RuH_3X (X = F, CH_3, and SiH_3). This material is available free of charge via the Internet at http://pubs.acs.org.

■ AUTHOR INFORMATION

Corresponding Author

*E-mail: odile.eisenstein@univ-montp2.fr (O.E.), christophe.raynaud@univ-montp2.fr (C.R.).

Notes

The authors declare no competing financial interest.

■ ACKNOWLEDGMENTS

The authors thank the CNRS, the Ministère de l'Enseignement Supérieur et de la Recherche (ANR) and the Agence Nationale de la Recherche for funding. They thank Drs. Marie-Liesse Doublet and Eric Clot (Montpellier) for useful discussions. A.I.P.-B. thanks the ANR project SIDERUS (ANR-08-Bla-0010-CSD3) for a postdoctoral fellowship. The authors thank IDRIS (project 100081) for a generous donation of computational time.

■ REFERENCES

(1) (a) Gillespie, R. J.; Nyholm, R. S. *Q. Rev.* **1957**, *11*, 339−380. (b) Gillespie, R. J.; Robinson, E. A. *Angew. Chem., Int. Ed. Engl.* **1996**, *35*, 495−514.

(2) (a) Demolliens, A.; Jean, Y.; Eisenstein, O. *Organometallics* **1986**, *5*, 1457−1464. (b) Kang, S. K.; Albright, T. A.; Eisenstein, O. *Inorg. Chem.* **1989**, *28*, 1613−1614. (c) Haaland, A.; Hammel, A.; Rypdal, K.; Volden, H. V. *J. Am. Chem. Soc.* **1990**, *112*, 4547−4549. (d) Shen, M. Z.; Schaefer, H. F., III.; Partridge, H. *J. Chem. Phys.* **1993**, *98*, 508−521. (e) Pfennig, V.; Seppelt, K. *Science* **1996**, *271*, 626−628. (f) Kaupp, M. *J. Am. Chem. Soc.* **1996**, *118*, 3018−5637. (g) Wang, X.; Andrews, L. *J. Am. Chem. Soc.* **2002**, *124*, 5636−5637. (h) Seppelt, K. *Acc. Chem. Res.* **2003**, *36*, 147−153.

(3) Kaupp, M. *Angew. Chem., Int. Ed.* **2001**, *40*, 3535−3565.

(4) Haaland, A.; Martinsen, K. G.; Shlykov, S. *Acta Chem. Scand.* **1992**, *46*, 1208−1210.

(5) Maseras, F.; Lledós, A.; Clot, E.; Eisenstein, O. *Chem. Rev.* **2000**, *100*, 601−636.

(6) Landis, C. R.; Cleveland, T.; Firman, T. K. *J. Am. Chem. Soc.* **1995**, *117*, 1859−1860.

(7) (a) Landis, C. R.; Firman, T. K.; Root, D. M.; Cleveland, T. *J. Am. Chem. Soc.* **1998**, *120*, 1842−1854. (b) Landis, C. R.; Weinhold, F. *J. Comput. Chem.* **2006**, *28*, 198−203.

(8) Weinhold, F.; Landis, C. R. *Valency and Bonding: A natural bond orbital donor-acceptor perspective*; Cambridge University Press: Cambridge, U.K., 2003.

(9) Landis, C. R.; Cleveland, T.; Firman, T. K. *J. Am. Chem. Soc.* **1998**, *120*, 2641−2649.

(10) Bayse, C. A.; Hall, M. B. *J. Am. Chem. Soc.* **1999**, *121*, 1348−1358.

(11) Stravopoulos, P.; Savage, P. D.; Tooze, R. P.; Wilkinson, G.; Hussain, B.; Motevalli, M.; Hursthouse, M. B. *J. Chem. Soc., Dalton Trans.* **1987**, 557−562.

(12) Savage, P. D.; Wilkinson, G.; Motevalli, M.; Hursthouse, M. B. *J. Chem. Soc., Dalton Trans.* **1988**, 669−673.

(13) Motherwell-Hay, R. S.; Wilkinson, G.; Hussain-Bates, B.; Hursthouse, M. B. *J. Chem. Soc., Dalton Trans.* **1992**, 3477−3482.

(14) Tooze, R. P.; Stavopoulos, P.; Motevalli, M.; Hursthouse, M. B.; Wilkinson, G. *J. Chem. Soc. Chem. Commun.* **1985**, 1139−1140.

(15) Frisch, M. J.; Trucks, G. W.; Schlegel, H. B.; Scuseria, G. E.; Robb, M. A.; Cheeseman, J. R.; Montgomery, Jr., J. A.; Vreven, T.; Kudin, K. N.; Burant, J. C.; Millam, J. M.; Iyengar, S. S.; Tomasi, J.; Barone, V.; Mennucci, B.; Cossi, M.; Scalmani, G.; Rega, N.; Petersson, G. A.; Nakatsuji, H.; Hada, M.; Ehara, M.; Toyota, K.; Fukuda, R.; Hasegawa, J.; Ishida, M.; Nakajima, T.; Honda, Y.; Kitao, O.; Nakai, H.; Klene, M.; Li, X.; Knox, J. E.; Hratchian, H. P.; Cross, J. B.; Bakken, V.; Adamo, C.; Jaramillo, J.; Gomperts, R.; Stratmann, R. E.; Yazyev, O.; Austin, A. J.; Cammi, R.; Pomelli, C.; Ochterski, J. W.; Ayala, P. Y.; Morokuma, K.; Voth, G. A.; Salvador, P.; Dannenberg, J. J.; Zakrzewski, V. G.; Dapprich, S.; Daniels, A. D.; Strain, M. C.; Farkas, O.; Malick, D. K.; Rabuck, A. D.; Raghavachari, K.; Foresman, J. B.; Ortiz, J. V.; Cui, Q.; Baboul, A. G.; Clifford, S.; Cioslowski, J.; Stefanov, B. B.; Liu, G.; Liashenko, A.; Piskorz, P.; Komaromi, I.; Martin, R. L.; Fox, D. J.; Keith, T.; Al-Laham, M. A.; Peng, C. Y.; Nanayakkara, A.; Challacombe, M.; Gill, P. M. W.; Johnson, B.; Chen, W.; Wong, M. W.; Gonzalez, C.; Pople, J. A. *Gaussian 03*, Revision C.02; Gaussian, Inc.: Wallingford, CT, 2004.

(16) (a) Perdew, J. P.; Wang, Y. *Phys. Rev. B* **1992**, *45*, 13244−13249. (b) Becke, A. D. *J. Chem. Phys.* **1993**, *98*, 5648−5652.

(17) (a) Ru and Rh: Peterson, K. A.; Figgen, D.; Dolg, M.; Stoll, H. *J. Chem. Phys.* **2007**, *126*, 124101−124112. (b) Re, Os and Ir: Figgen, D.; Peterson, K. A.; Dolg, M.; Stoll, H. *J. Chem. Phys.* **2009**, *130*, 164108−164112.

(18) Hariharan, P. C.; Pople, J. A. *Theor. Chim. Acta* **1973**, *28*, 213−222.

(19) Adamo, C.; Barone, V. *J. Chem. Phys.* **1999**, *110*, 6158−6169.

(20) Weigend, F.; Ahlrichs, R. *Phys. Chem. Chem. Phys.* **2005**, *7*, 3297−3305.

(21) Andrae, D.; Häussermann, U.; Dolg, M.; Stoll, H.; Preuss, H. *Theor. Chim. Acta* **1990**, *77*, 123−141.

(22) Werner, H.-J.; Knowles, P. J.; Knizia, G.; Manby, F. R.; Schütz, M.; Celani, P.; Korona, T.; Lindh, R.; Mitrushenkov, A.; Rauhut, G.; Shamasundar, K. R.; Adler, T. B.; Amos, R. D.; Bernhardsson, A.; Berning, A.; Cooper, D. L.; Deegan, M. J. O.; Dobbyn, A. J.; Eckert, F.; Goll, E.; Hampel, C.; Hesselmann, A.; Hetzer, G.; Hrenar, T.; Jansen, G.; Köppl, C.; Liu, Y.; Lloyd, A. W.; Mata, R. A.; May, A. J.; McNicholas, S. J.; Meyer, W.; Mura, M. E.; Nicklass, A.; O'Neill, D. P.; Palmieri, R.; Pflüger, K.; Pitzer, R.; Reiher, M.; Shiozaki, T.; Stoll, H.; Stone, A. J.; Tarroni, R.; Thorsteinsson, T.; Wang, M.; Wolf, A. *MOLPRO*, version 2010.1; see http://www.molpro.net.

(23) Toulouse, J.; Colonna, F.; Savin, A. *J. Chem. Phys.* **2005**, *122*, 014110.

(24) Gerber, I. C.; Ángyán, J. G. *J. Chem. Phys.* **2007**, *126*, 044103.

(25) Weigend, F.; Furche, F.; Ahlrichs, R. *J. Chem. Phys.* **2003**, *119*, 12753.

(26) Neese, F. *Orca: an ab initio, Density Functional and Semiempirical program package*, version 2.9; MPI für Bioanorganische Chemie: Mülheim, Germany, 2012.

(27) Gdanitz, R. J. *Int. J. Quantum Chem.* **2001**, *85*, 281−300.

(28) (a) Hättig, C. *Phys. Chem. Chem. Phys.* **2005**, *7*, 59−66. (b) Hellweg, A.; Hättig, C.; Höfener, S.; Klopper, W. *Theor. Chem. Acc.* **2007**, *117*, 587−597.

(29) *YAeHMOP*, version 3.0; yaehmop-help@lists.sourceforge.net.

(30) Thorn, D. L.; Hoffmann, R. *Inorg. Chem.* **1978**, *17*, 126−140.

(31) (a) Reed, A. E.; Curtiss, L. A.; Weinhold, F. *Chem. Rev.* **1988**, *88*, 899−926. (b) Glendening, E. D.; Badenhoop, J. K.; Reed, A. E.; Carpenter, J. E.; Bohmann, J. A.; Morales, C. M.; Weinhold, F. *NBO*, 5.0; Theoretical Chemistry Institute, University of Wisconsin, Madison, WI, 2001.
(32) Root, D. M.; Landis, C. R.; Cleveland, T. *J. Am. Chem. Soc.* **1993**, *115*, 4201−4209.
(33) (a) Lee, T. J.; Taylor, P. R. *Int. J. Quantum Chem.* **1989**, *36* (S23), 199−207. (b) Janssen, C. L.; Nielsen, I. M. B. *Chem. Phys. Lett.* **1998**, *290*, 423−430.
(34) Jiang, W.; DeYonker, N. J.; Wilson, A. K. *J. Chem. Theory Comput.* **2012**, *8*, 460−468.
(35) Bondi, A. *J. Phys. Chem.* **1964**, *68*, 441−451.
(36) (a) Besora, M.; Maseras, F.; Lledós, A.; Eisenstein, O. *Inorg. Chem.* **2002**, *41*, 7105−7112. (b) Besora, M.; Maseras, F.; Lledós, A.; Eisenstein, O. *Organometallics* **2006**, *25*, 4748−4755.
(37) Weinhold, F.; Landis, C. R. *Valency and Bonding: A natural bond orbital donor-acceptor perspective*; Cambridge University Press: Cambridge, U.K., 2003; p 390.
(38) (a) Glendening, E. D.; Weinhold, F. *J. Comput. Chem.* **1998**, *19*, 593−609. (b) Glendening, E. D.; Weinhold, F. *J. Comput. Chem.* **1998**, *19*, 610−627. (c) Glendening, E. D.; Badenhoop, J. K.; Weinhold, F. *J. Comput. Chem.* **1998**, *19*, 628−646.
(39) The percentages shown in Figure 11 include the contribution of equivalent hydrogens.
(40) Lachaize, S.; Sabo-Etienne, S. *Eur. J. Inorg. Chem.* **2006**, *11*, 2115−2127.
(41) Nikonov, G. I. *Adv. Organomet. Chem.* **2005**, *53*, 217−309.